Seismic Forward Problem:
Numerical Solutions

Qinya Liu

University of Toronto

USTC, May 2020

Forward Problem is the key to all inverse problems

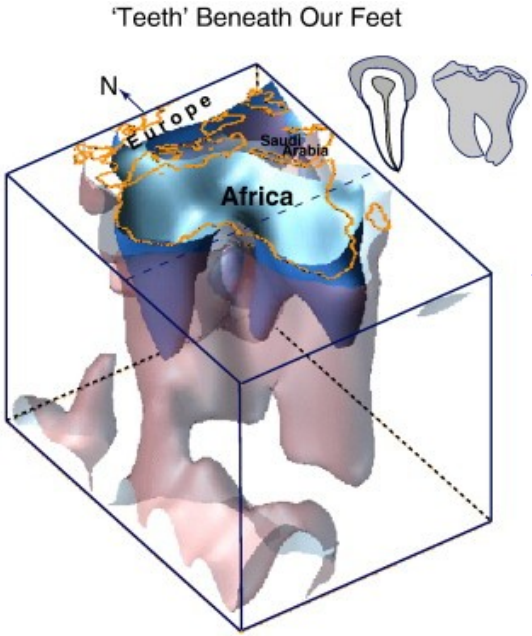

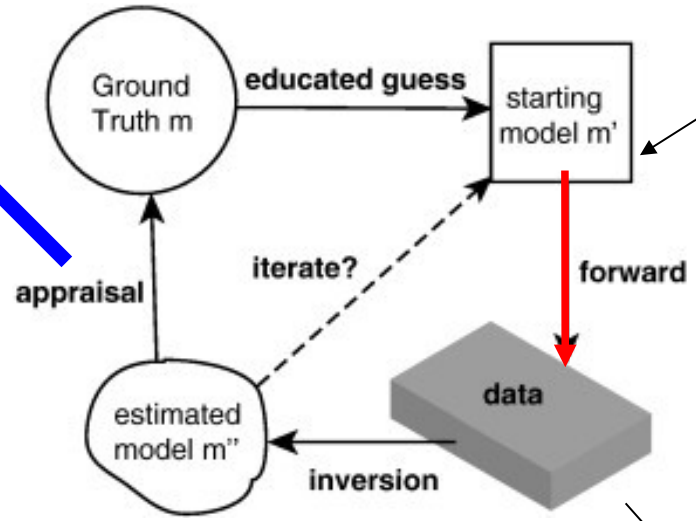

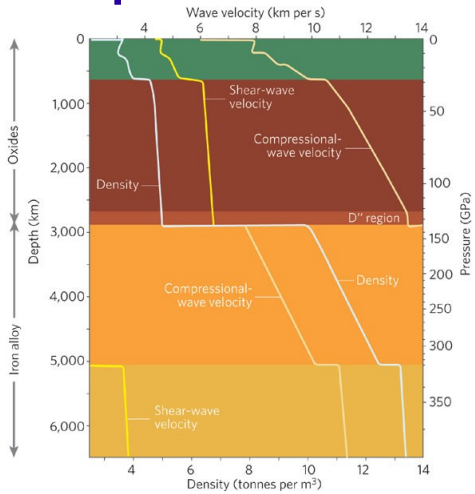

Dziewonski & Anderson 1981

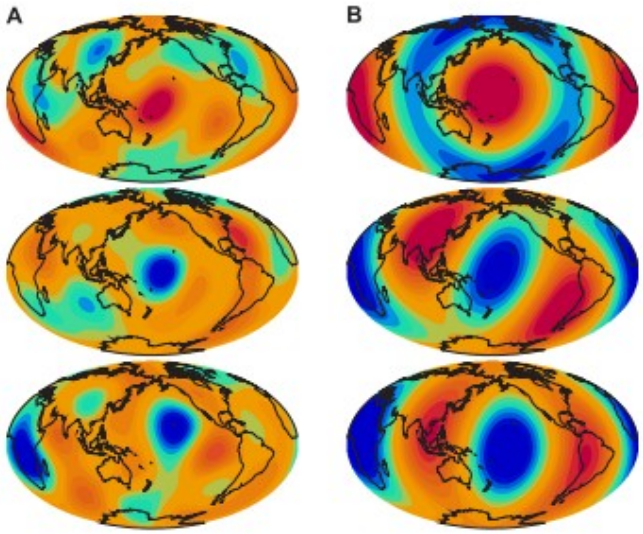

Vs

Vb

rho

Ishii & Tromp (1999)

Stein & Wysession 2003

Figure 2.7-1: Seismograms recorded at a distance of 110°, showing surface waves.

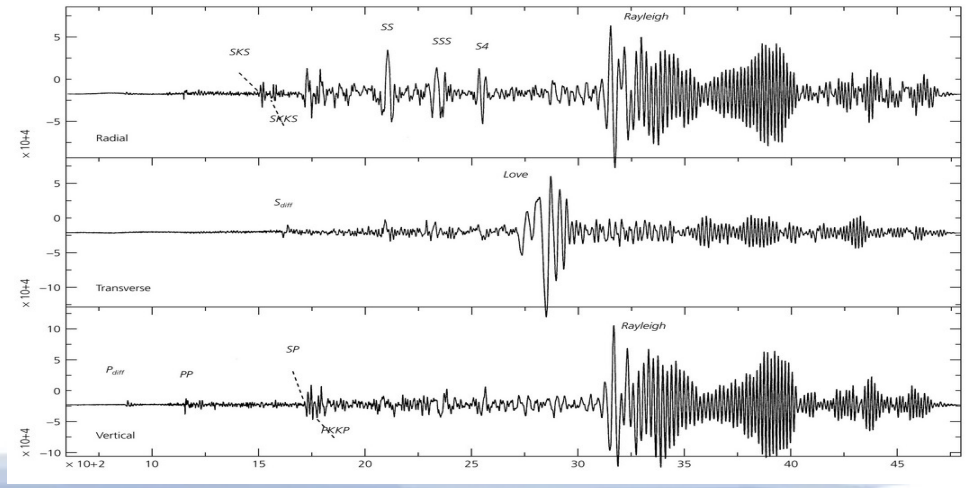

Seismic Frequency Bands

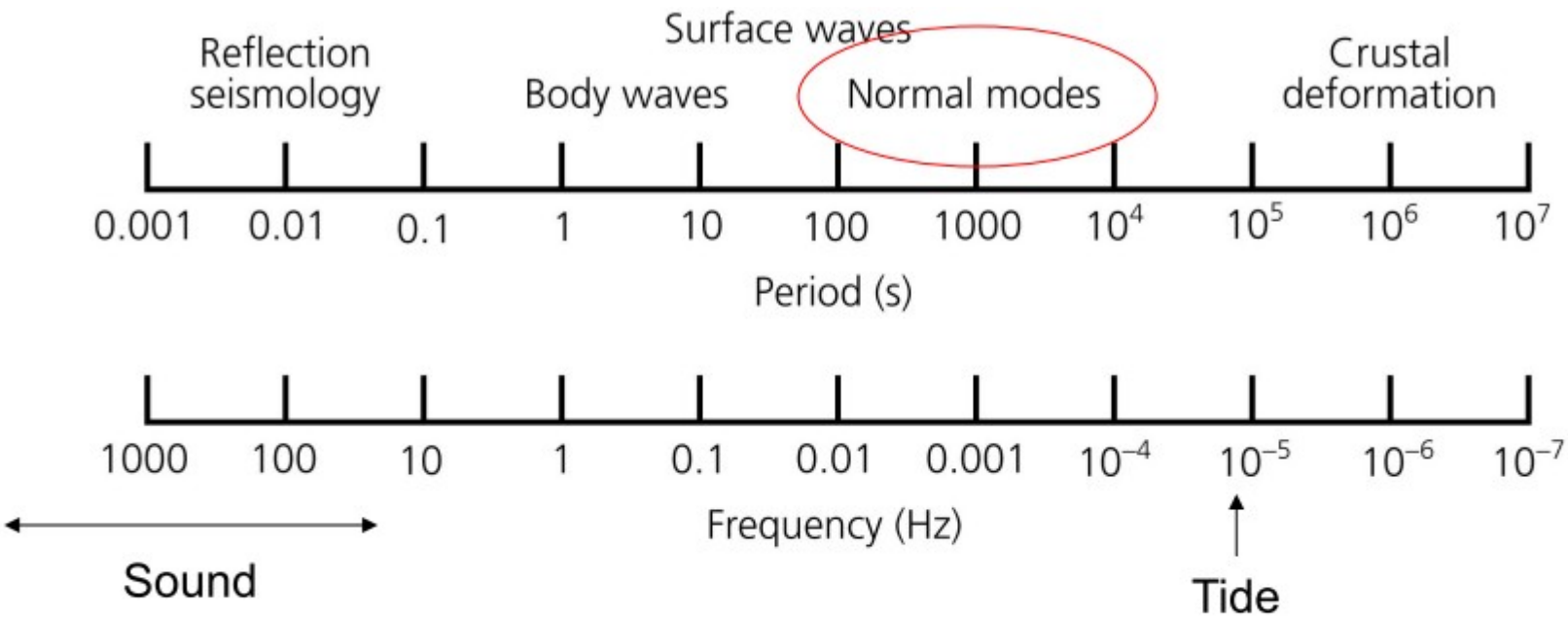

Stein & Wysession (2003)

The elastodynamic equation

Elastodynamics PDEs

$$\rho \partial_t^2 \mathbf{s} = \nabla \cdot \mathbf{T} + \mathbf{f} \quad \text{in } \Omega$$

where the stress is related to strain based on the linear constitutive relation

$$\mathbf{T} = \mathbf{C} : \epsilon = \mathbf{C} : \nabla \mathbf{s}$$

and the wavefield satisifies the free surface boundary condition

$$\hat{n} \cdot \mathbf{T} = 0 \quad \text{on } \partial\Omega$$

and initial condition

$$\mathbf{s}(\mathbf{x}, t = 0) = 0, \quad \dot{\mathbf{s}}(\mathbf{x}, t = 0) = 0.$$

How would you solve this PDE by numerical methods?

Finite-difference

For one-dimensional wave propagation (or two-dimensional SH wave propagation, $\mathbf{u} = (0, u, 0)$)

$$\rho(x)\frac{\partial^2 u}{\partial t^2} = \frac{\partial}{\partial x}\left[\mu(x)\frac{\partial u}{\partial x}\right] \tag{24}$$

First use the stress-velocity formulation to obtain a first-order PDE system

$$\frac{\partial \sigma}{\partial t} = \mu(x)\frac{\partial \dot{u}}{\partial x}, \quad \frac{\partial \dot{u}}{\partial t} = \frac{1}{\rho}\frac{\partial \sigma}{\partial x}$$

Discretization of derivatives: use central-difference formula

$$\frac{\partial f}{\partial x}\Big|_x = \frac{1}{2\Delta x}\left[f(x+\Delta x) - f(x-\Delta x)\right] + O[(\Delta x)^2] \tag{25}$$

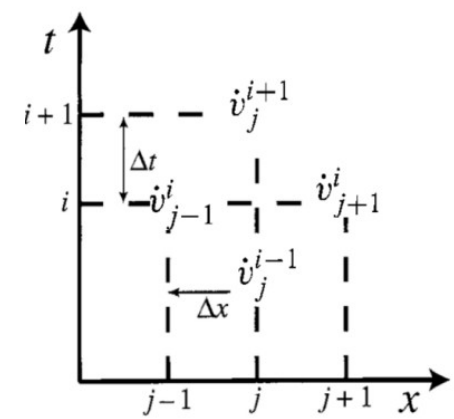

$$\frac{\partial \dot{u}}{\partial t} = \frac{1}{\rho}\frac{\partial \sigma}{\partial x}, \quad \frac{\partial \sigma}{\partial t} = \mu(x)\frac{\partial \dot{u}}{\partial x} \tag{26}$$

become

$$\begin{aligned} \frac{\dot{u}_j^{i+1} - \dot{u}_j^{i-1}}{2\Delta t} &= \frac{1}{\rho_j}\frac{\sigma_{j+1}^i - \sigma_{j-1}^i}{2\Delta x} \\ \frac{\sigma_j^{i+1} - \sigma_j^{i-1}}{2\Delta t} &= \mu_j\frac{\dot{u}_{j+1}^i - \dot{u}_{j-1}^i}{2\Delta x} \end{aligned} \tag{27}$$

Staggered-grid Finite-difference Methods

3D

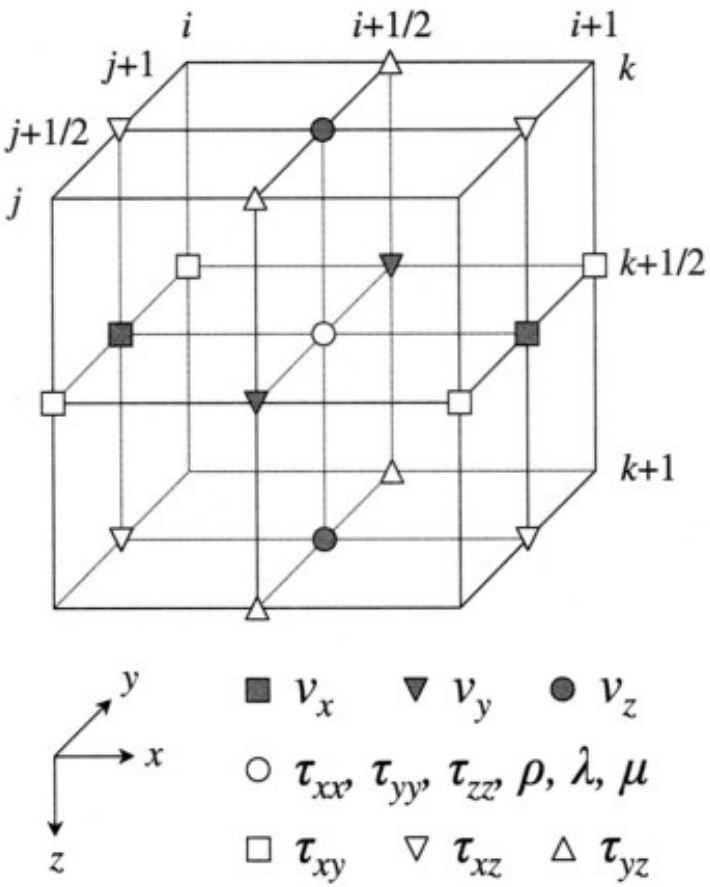

2D

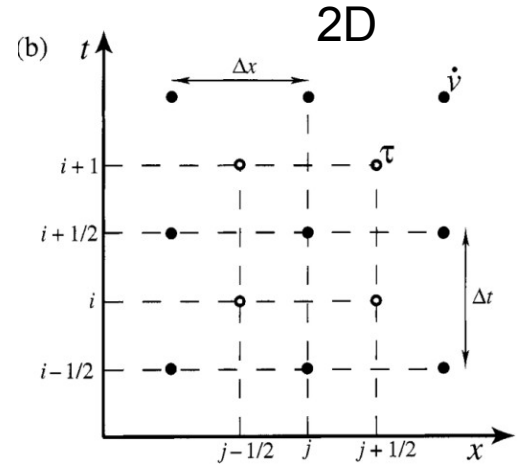

Using Taylor Series Expansions we found the following finite-differences equations

$$f'(x_i) \approx \frac{f(x_{i+1}) - f(x_i)}{h} + O(h)$$ FORWARD DIFFERENCE

$$f'(x_i) \approx \frac{f(x_i) - f(x_{i-1})}{h} + O(h)$$ BACKWARD DIFFERENCE

$$f'(x_i) \approx \frac{f(x_{i+1}) - f(x_{i-1})}{2h} + O(h^2)$$ CENTRAL DIFFERENCE

$$f''(x_i) \approx \frac{f(x_{i+1}) - 2f(x_i) + f(x_{i-1})}{h^2} + O(h^2)$$ CENTRAL DIFFERENCE

Finite-difference Methods

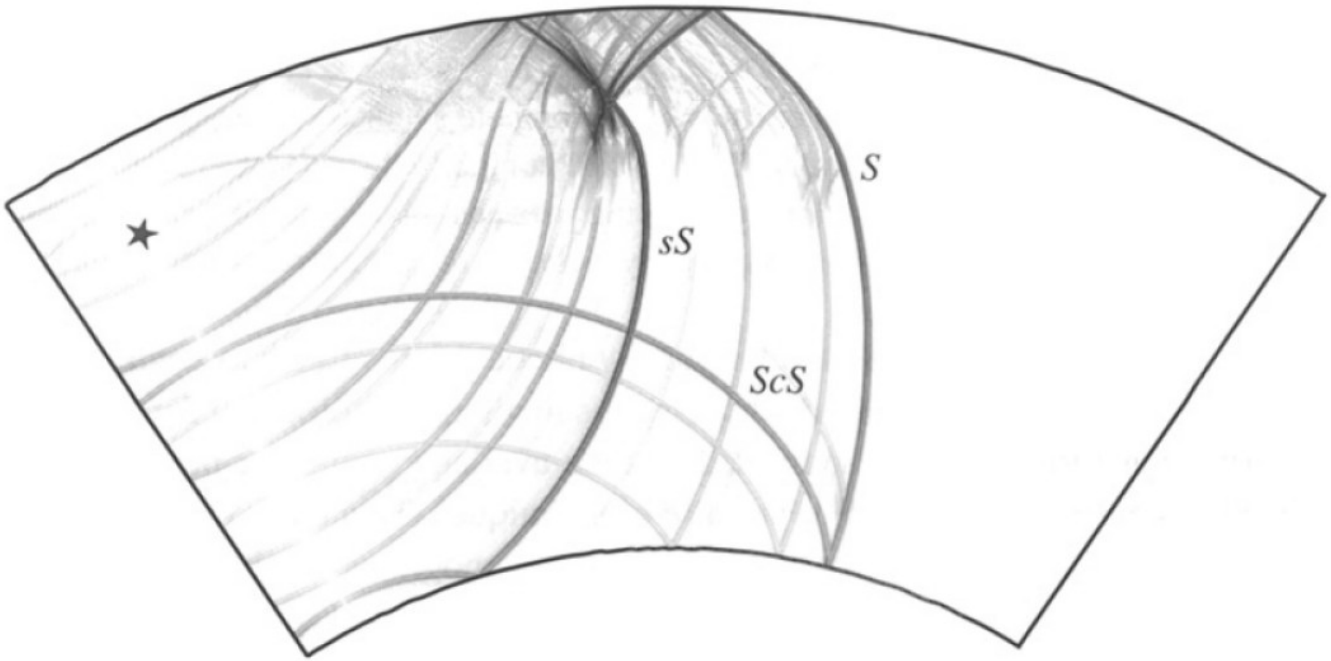

Figure 3.3 The *SH*-velocity wavefield in the mantle after 10 minutes for a source at 500 km depth (star), adapted from a figure in Thorne *et al.* (2007). This axi-symmetric 2-D finite-difference calculation used the PREM velocity model. The major seismic phases are labeled (see Chapter 4); the lower amplitude phases are mainly reflections off upper-mantle discontinuities and an assumed discontinuity 264 km above the core--mantle boundary.

Adjoint tomography: 3D numerical solvers

- Finite difference
- Finite element
- Spectral element

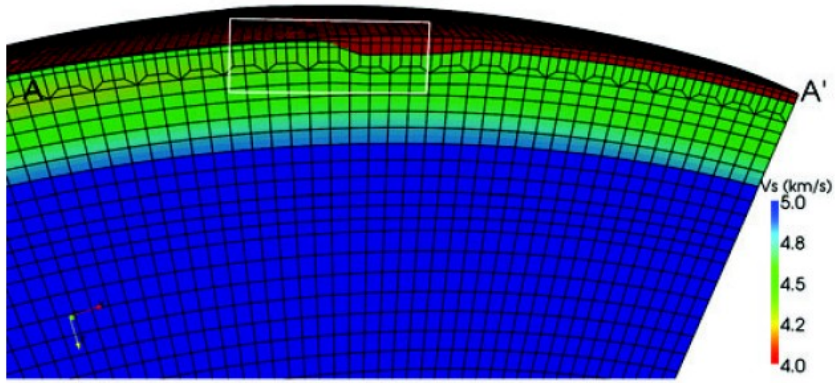

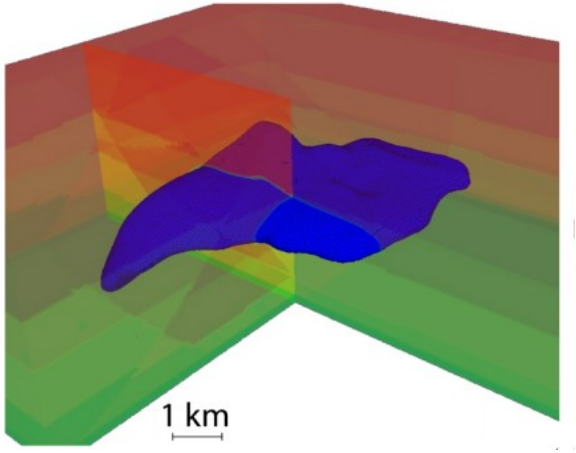

SPECFEM3D_GLOBE
Komatitsch & Tromp (2002 a, b), Tromp et al (2010)

SPECFEM3D,
Komatitsch et al (2004), Peter et al (2011)

Advantages:

* Weak formulation → topography, internal surfaces, complex geology

* Interpolation/integration of wavefield on local GLL points → diagonal mass matrix

* Meshing by doubling schemes → efficient

* Diagonal mass matrix, local communications → Parallel computation

* Community-supported/developed, open-source; GPU-enabled.

Computational Infrastructure for Geodynamics (CIG):
http://www.geodynamics.org/cig/software/packages/seismo/

Accuracy of SEM

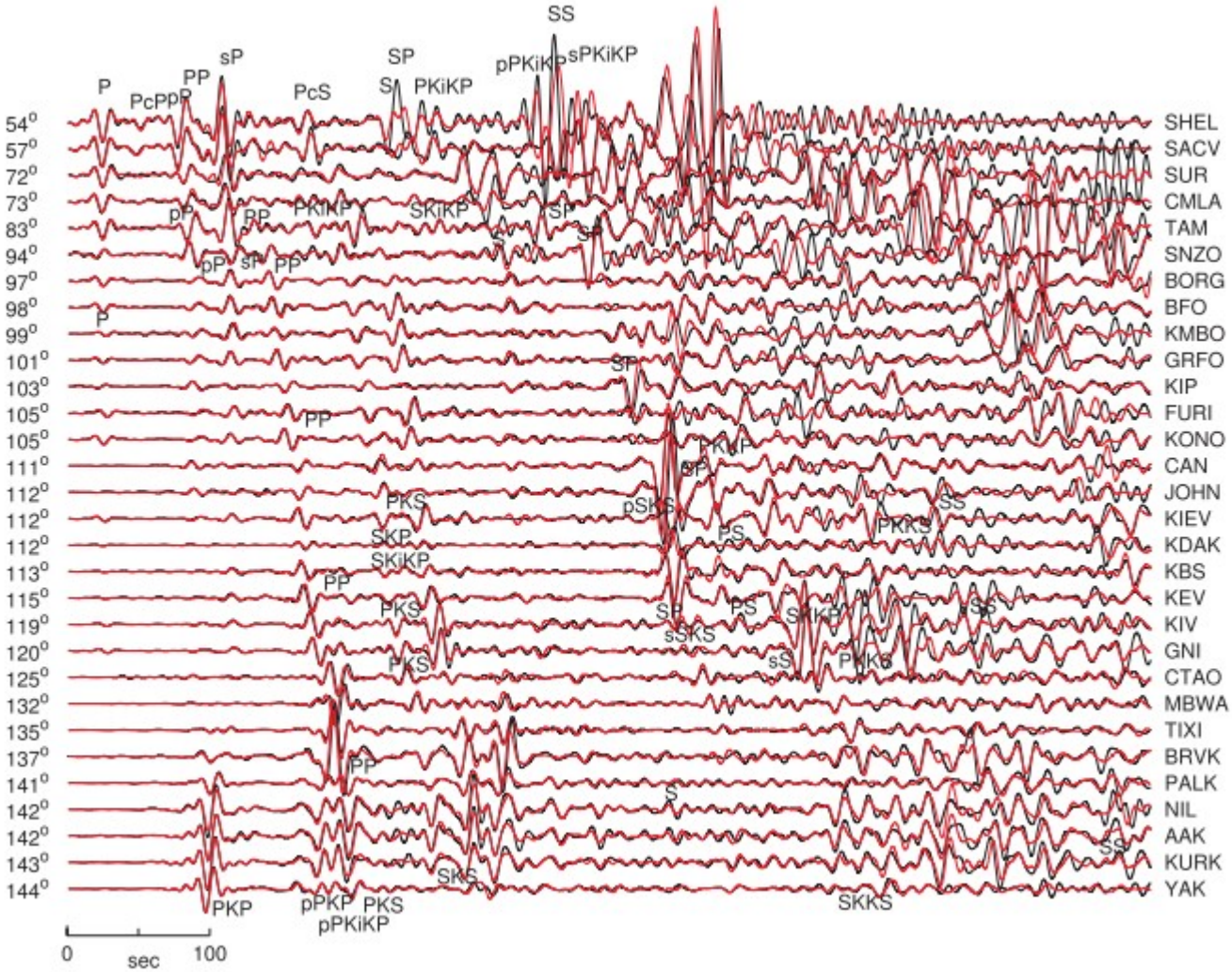

Z-comp record section between data (black) and SEM synthetics (red) for the 2008 September 3, Mw = 6.3 Santiago del Estero, Argentina earthquake (depth=571 km)

http://global.shakemovie.princeton.edu/

Tromp et al (2010)

Introduction to Spectral-element Methods

Theory, Implementation and Applications

May 29, 2020

Finite-difference method

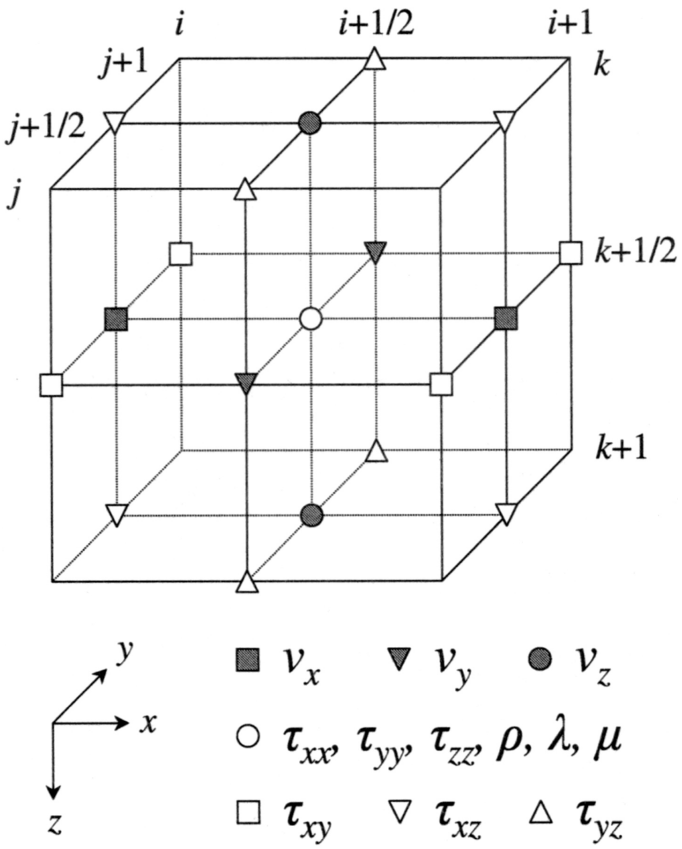

Using Taylor Series Expansions we found the following finite-differences equations

$$f'(x_i) \approx \frac{f(x_{i+1}) - f(x_i)}{h} + O(h)$$ FORWARD DIFFERENCE

$$f'(x_i) \approx \frac{f(x_i) - f(x_{i-1})}{h} + O(h)$$ BACKWARD DIFFERENCE

$$f'(x_i) \approx \frac{f(x_{i+1}) - f(x_{i-1})}{2h} + O(h^2)$$ CENTRAL DIFFERENCE

$$f''(x_i) \approx \frac{f(x_{i+1}) - 2f(x_i) + f(x_{i-1})}{h^2} + O(h^2)$$ CENTRAL DIFFERENCE

Finite-element method: History

FEM is considered a milestone in computational mathematics.

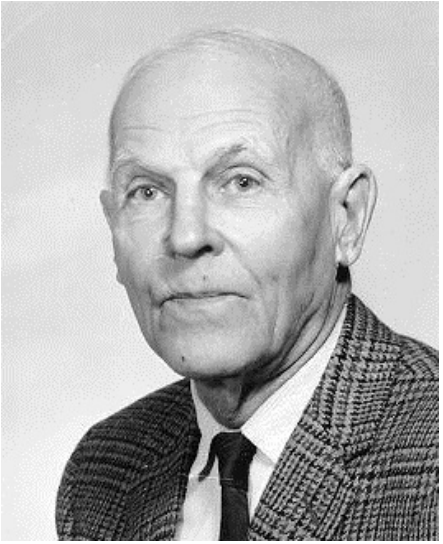

(a)

(b)

(c)

Alexander Hrennikoff (1896-1984), lattice model (1941) leading to the development of FEM; **Richard Courant** (1888-1972), triangular elements (1943); **Feng Kang** (1920-1993): finite difference method based on variation principle (late 1950 to early 1960)
Significant development in the 1960-1970 due to the advancement of computation power

Finite-element method

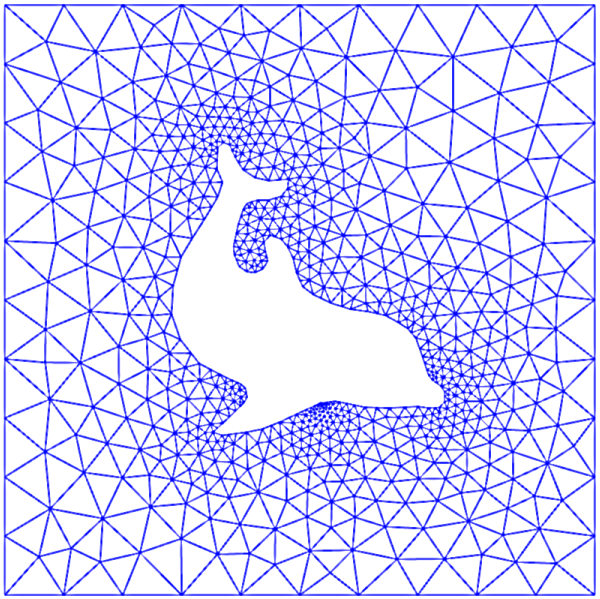

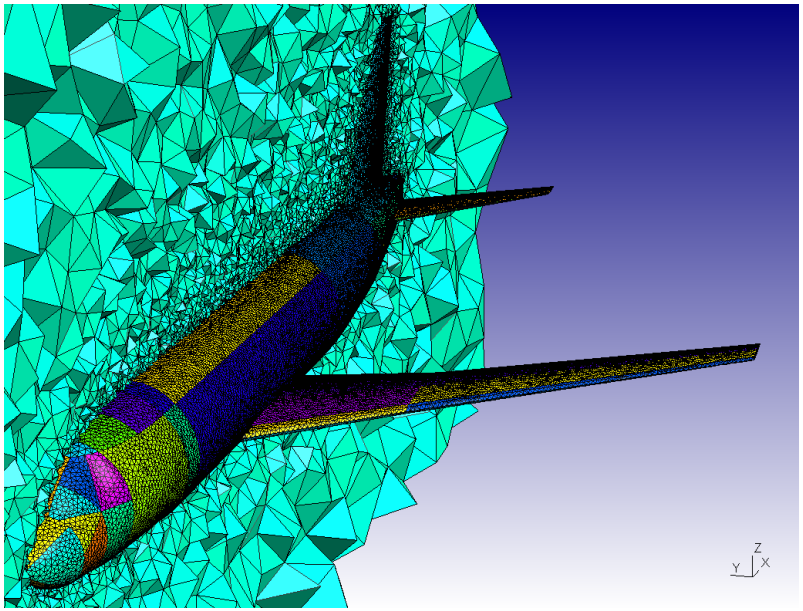

FEM mesh can be used to accurately describe complex model geometry, mostly with triangular or tetrahedral elements

Meshing in 2D and 3D

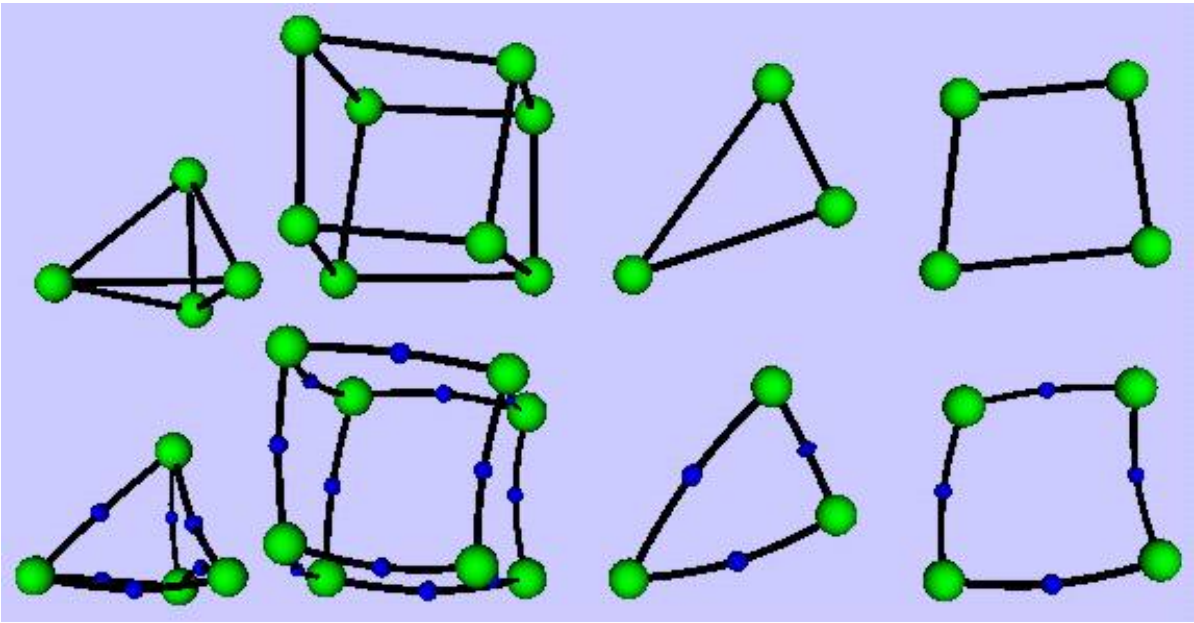

Meshing in 2D: triangular vs quadrilateral mesh; in 3D tetrahedral mesh vs hexahedral mesh

SEM Meshing

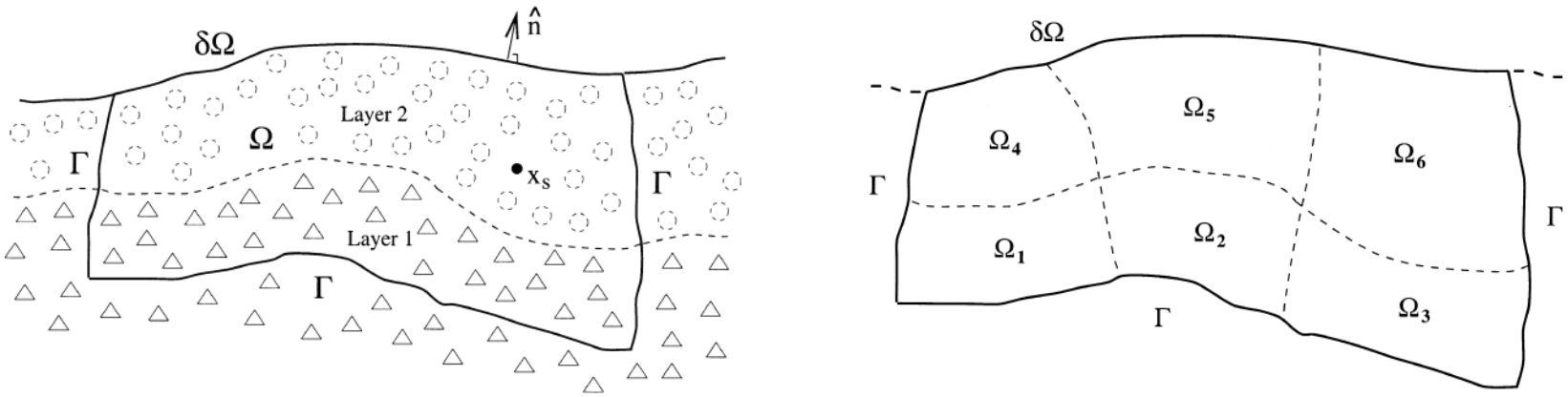

Figure: Meshing a simulation domain Ω with free surface boundary $\delta\Omega$ and possibly artificial boundary Γ; Resulting 2D quadrilateral mesh in 2D and hexhedral mesh in 3D conform to external and internal discontinuities

SEM anchors for Shape functions

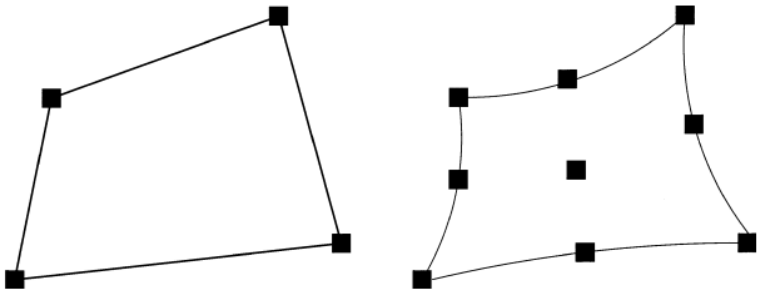

Figure: N_e=2 vs $N_e = 3$ for quadrilateral elements

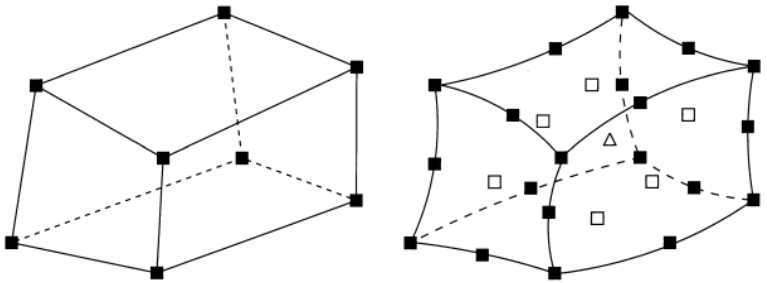

Figure: N_e=2 vs $N_e = 3$ for hexhedral elements

SEM GLL points for wavefield

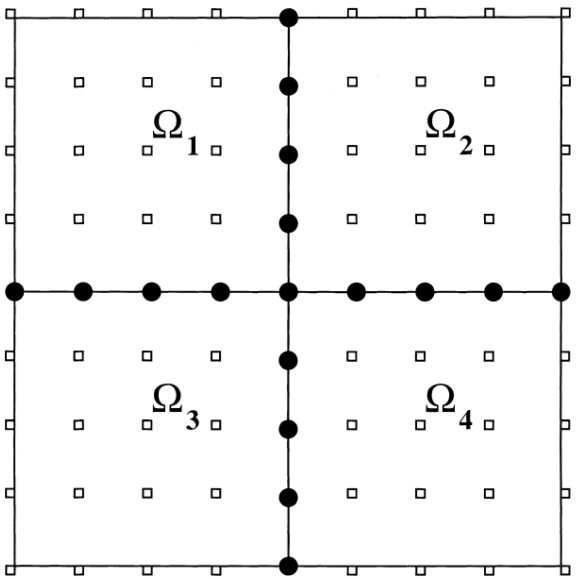

Figure: 2D SEM mesh with $NGLL = 4$

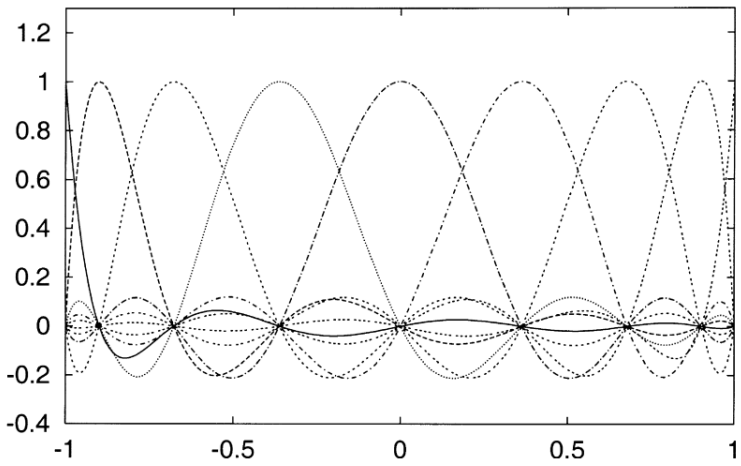

Figure: Langrange polynomial for GLL points with $NGLL = 8$

SEM uses the same set of Gauss-Lobatto-Legendre (GLL) points defined by $(1 - \xi^2)P'_N(\xi) = 0$ as interpolation and integration points

Mesh doubling in 3D

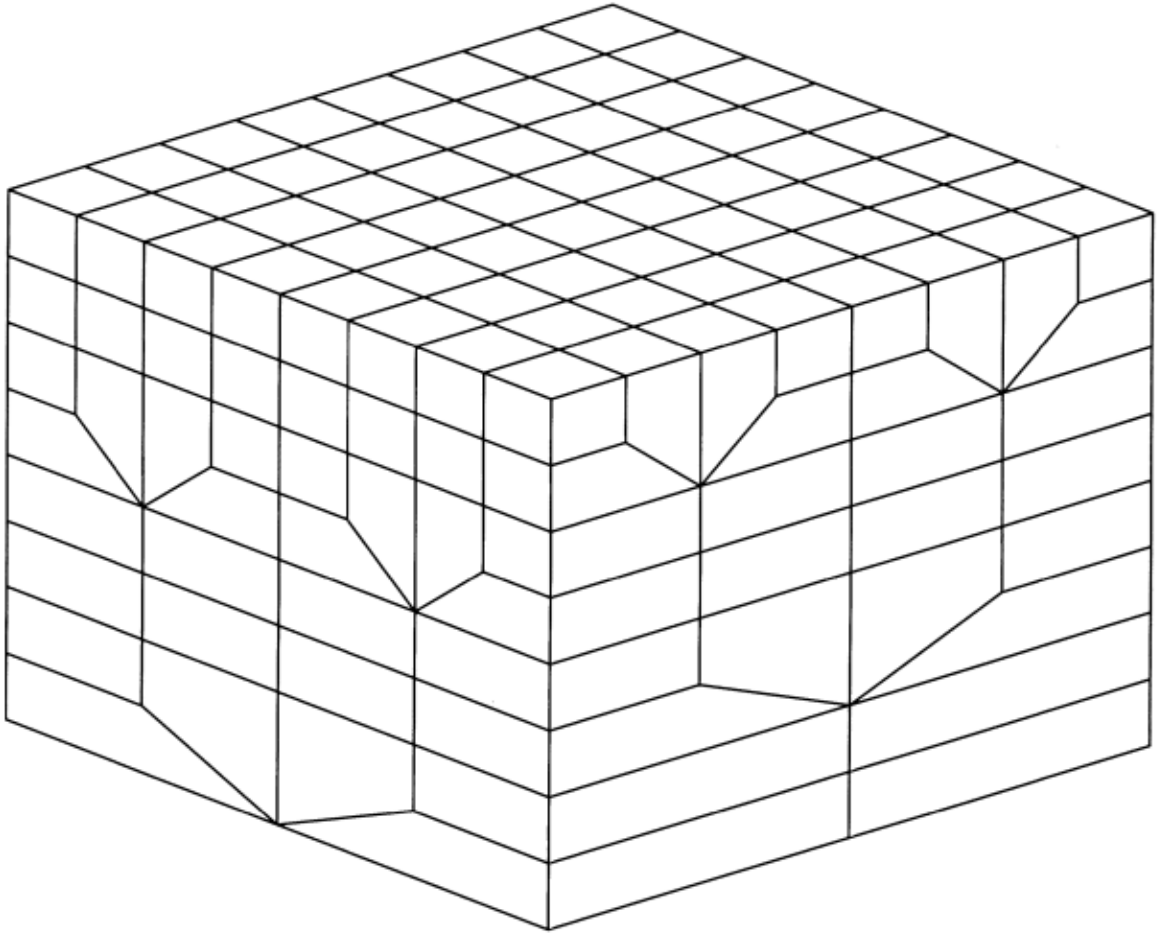

Figure: From 8X8 elements on the surface to 2X2 elements at the bottom

SEM packages

Figure: Accessed through GitHub website

High performance Computer

Figure: The TCS machine at SciNet, one of the state-of-the-art HPC in Canada.

SEM for the globe

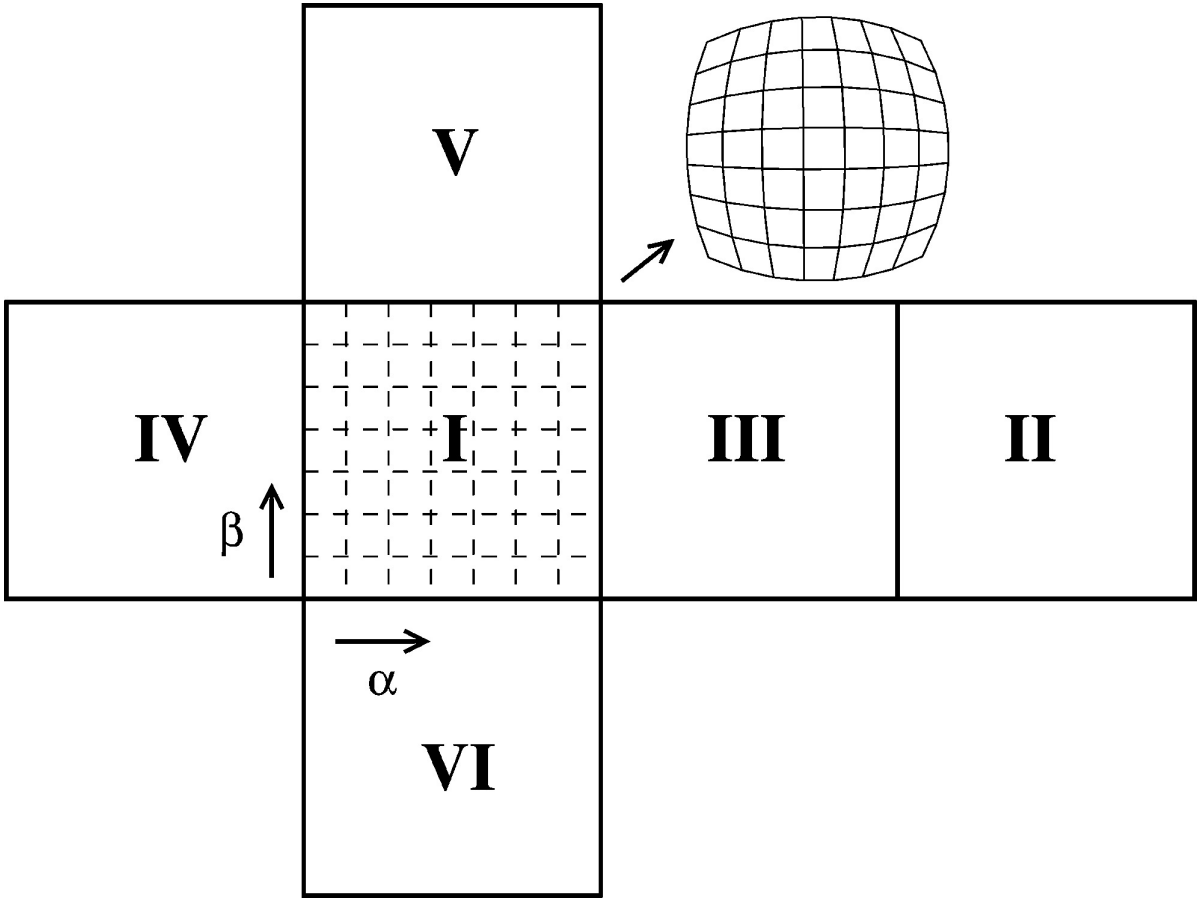

Figure: The globe is divided into 6 chunks, 4 along the equator and one at the north/south pole respectively

A cube in the centre

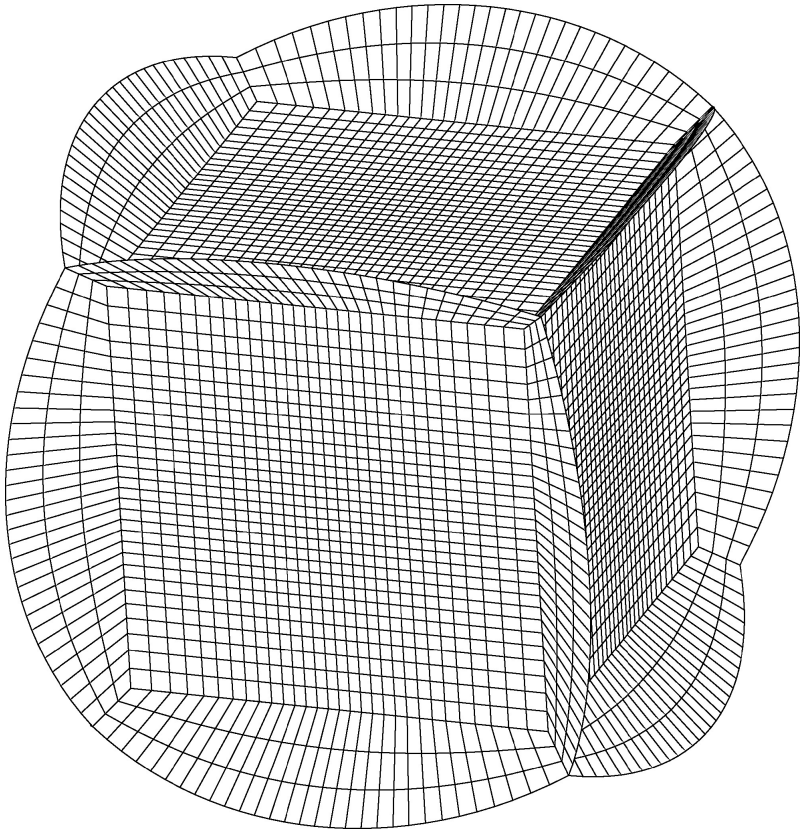

Figure: To avoid singularity at the centre, a cube is placed in the inner core (3 layer of elements down from ICB) with mesh from simple interpolation.

Mesh doubling

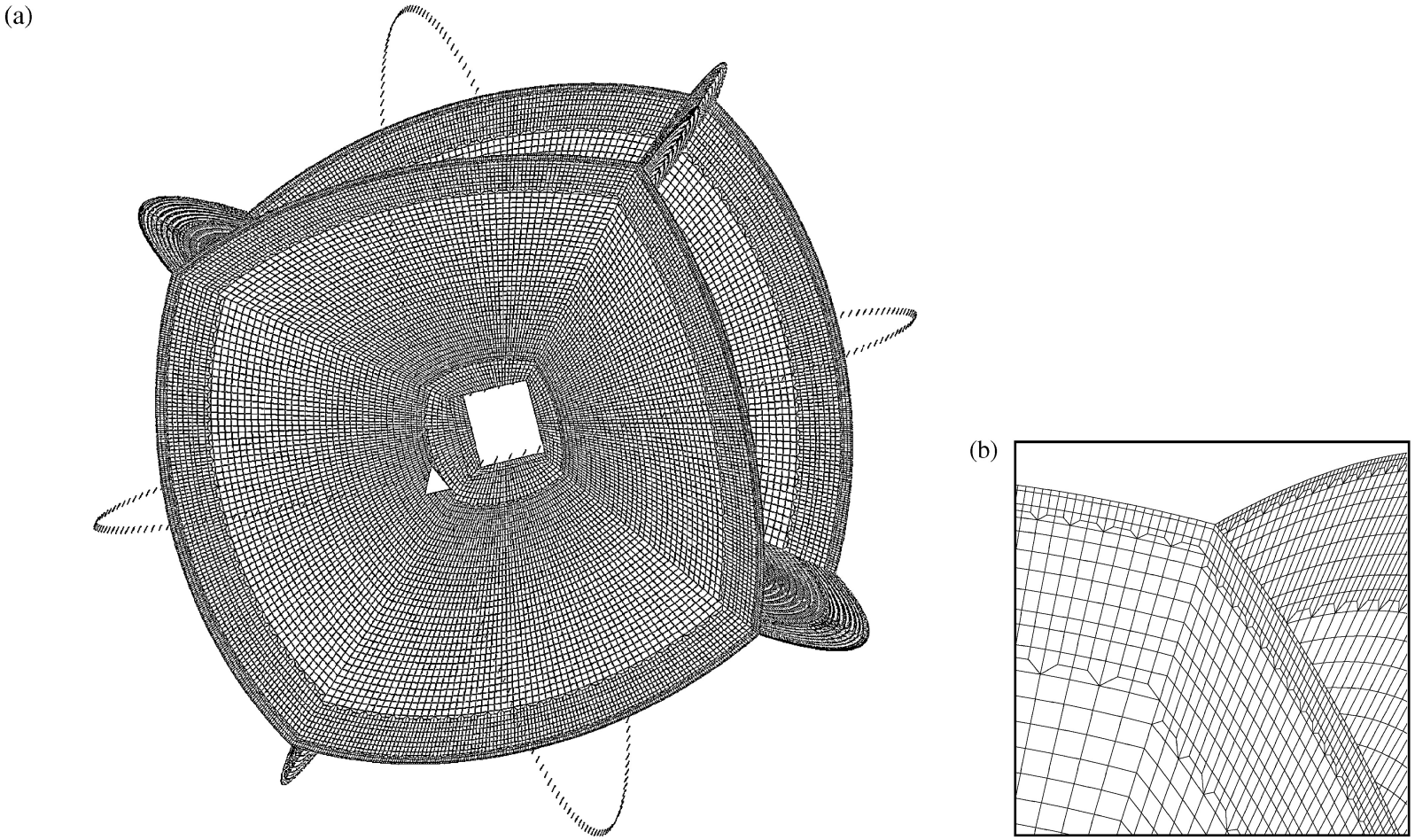

Figure: Mesh doubling beneath Moho and 660 km discontinutity and once in the outer core just above ICB.

Stability condition for the global code

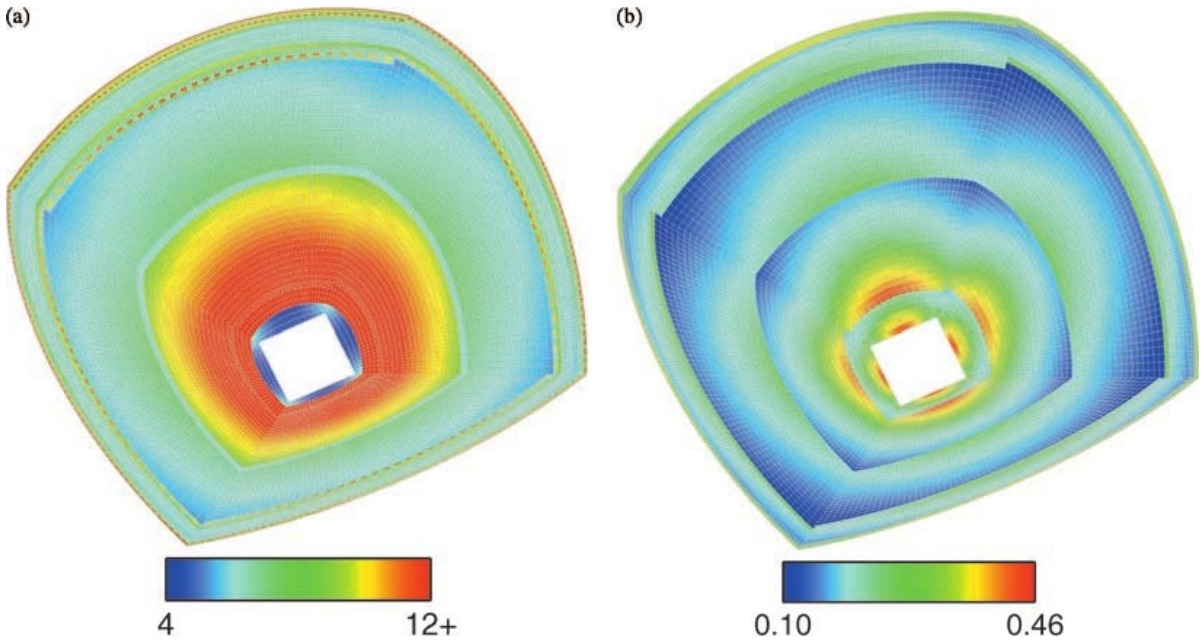

Figure: (left) Number of points per wavelength (right) Courant number

Parallel implementation for the globe

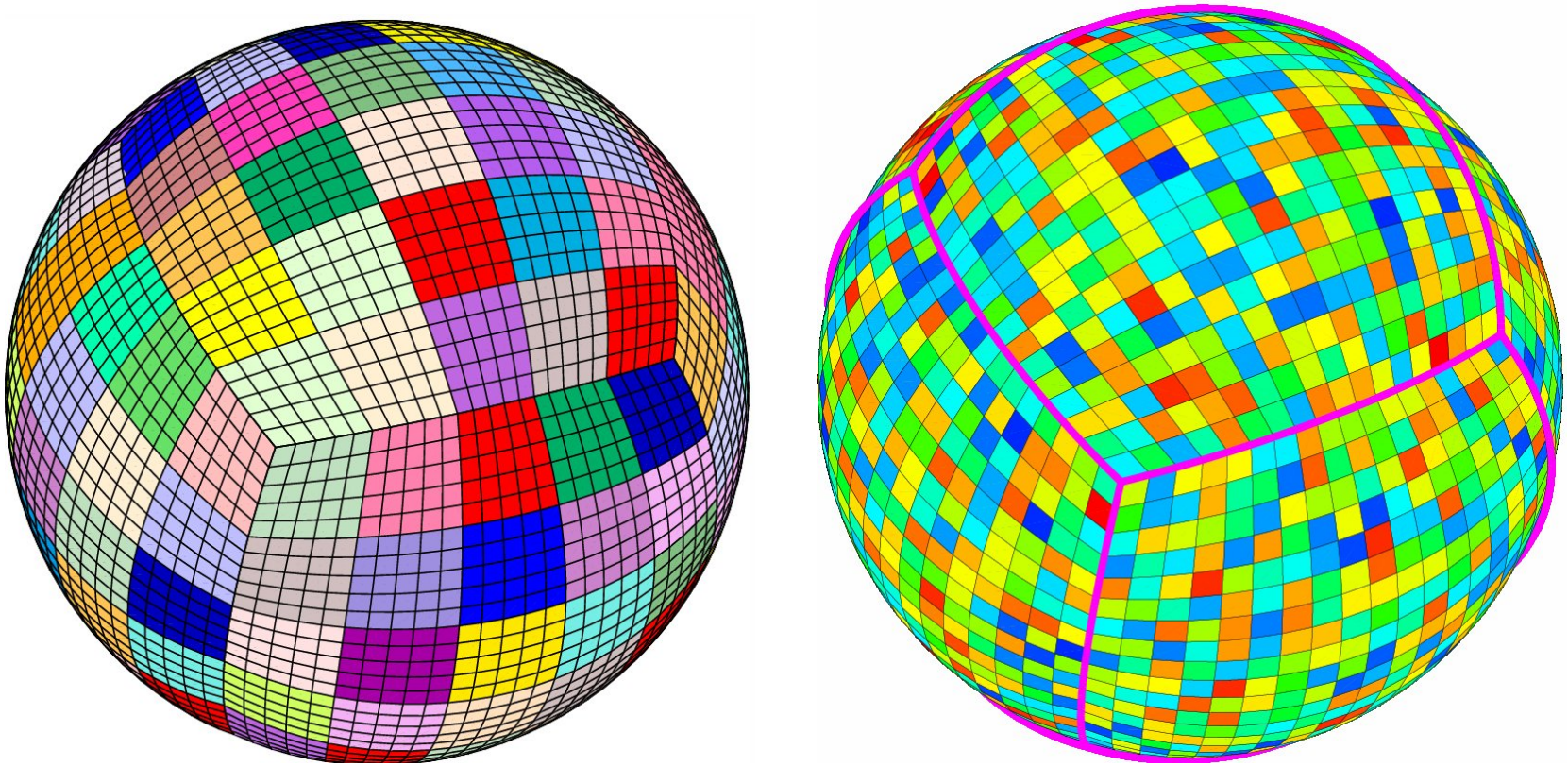

Figure: MPI slices for SEM parallel simulations (left $6X5X5$; right $6X18X18$). Computation on each slice is performed on one core (process).

the global S20RTS model

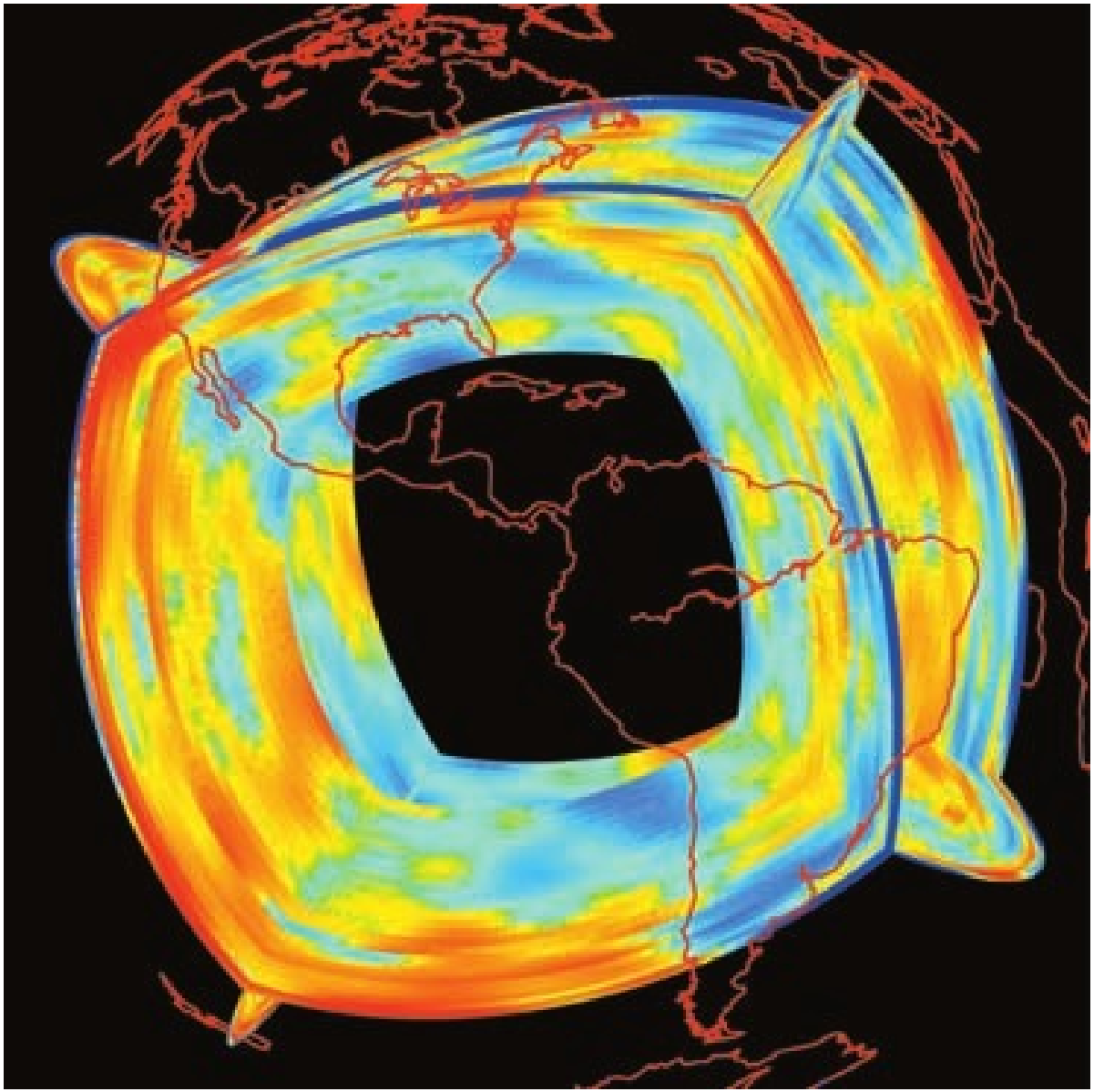

Waveform fits for 3D global models vs. 1D PREM

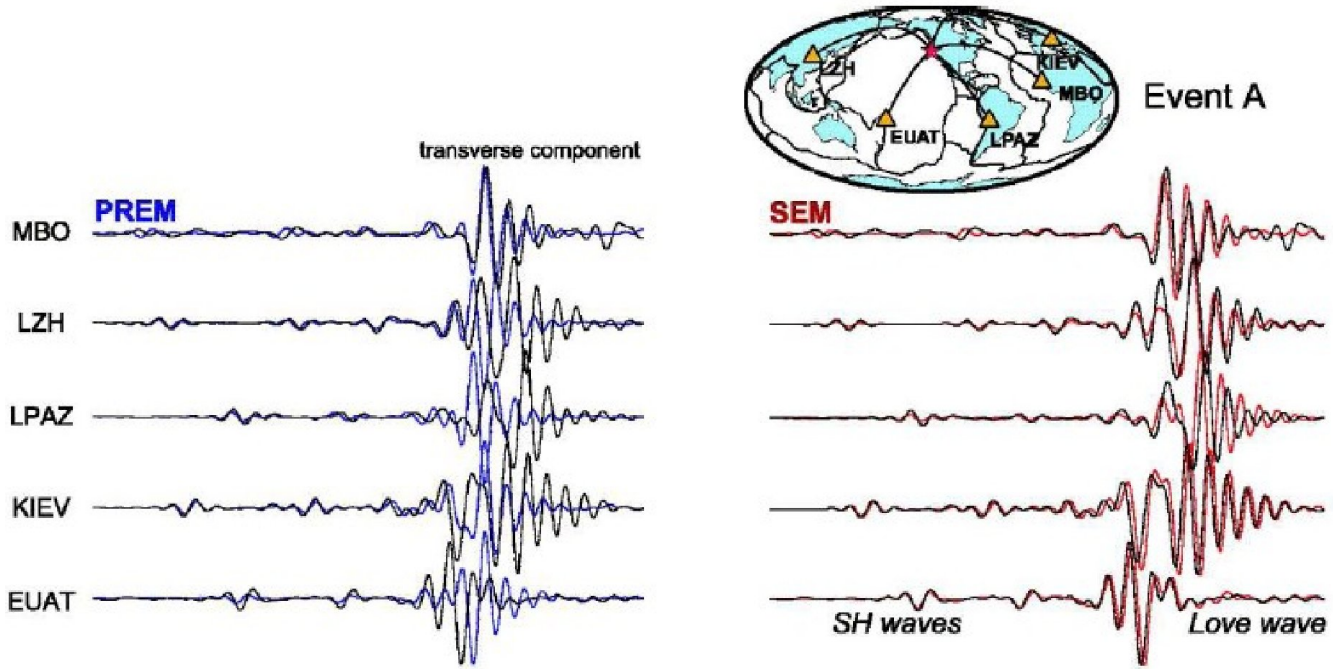

Feb 19, 1995, $M_w = 6.6$, off-shore California Earthquake
transvserse components, 50 seconds and longer
Komatitsch et al. (2002)

SPECFEM3D: Challenges in Meshing

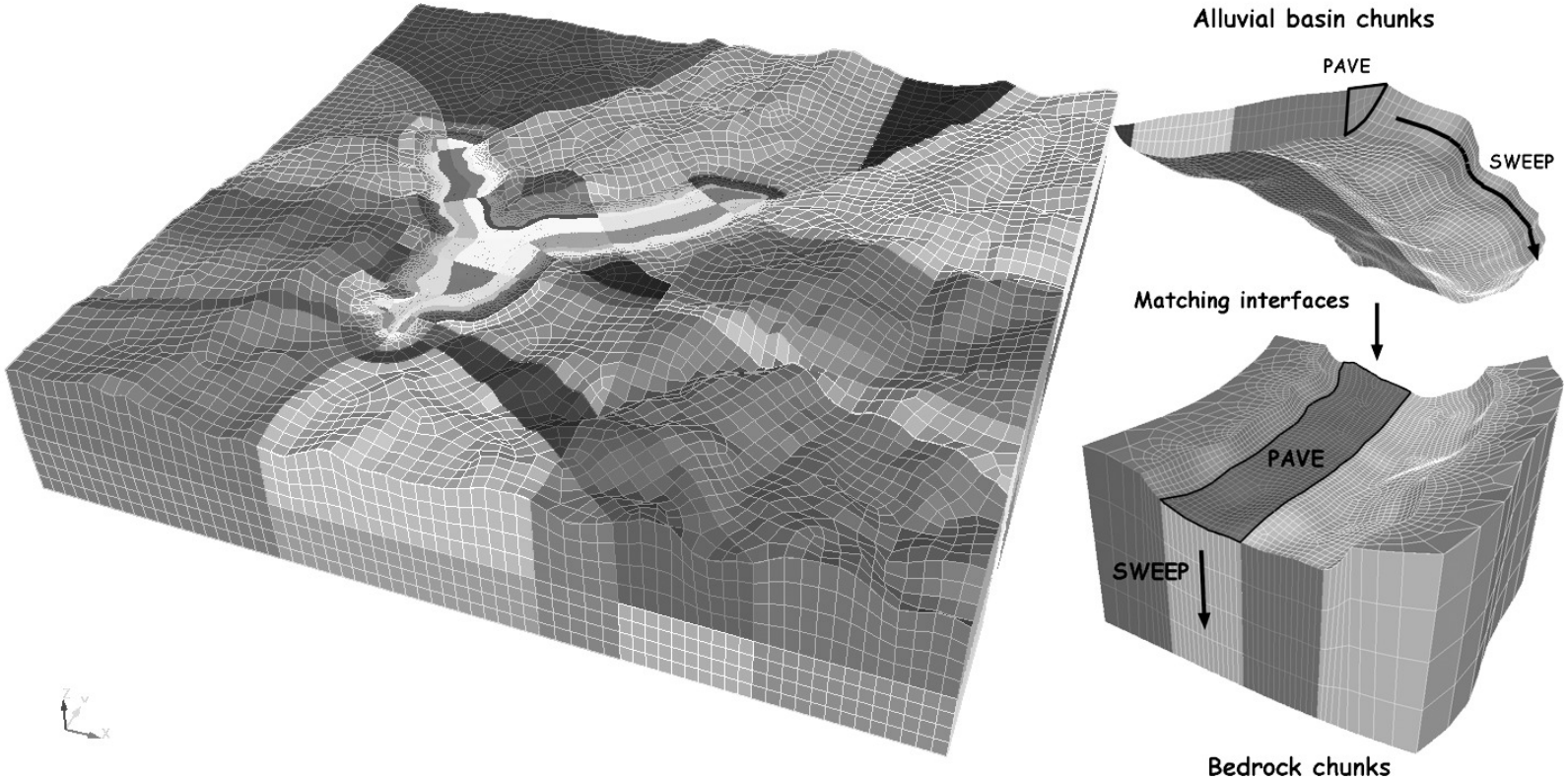

Figure: Hexhedral meshing including a alluvial basin